Applied Water Science (2023) 13:44
https://doi.org/10.1007/s13201-022-01852-8

ORIGINAL ARTICLE

4E investigation of solar-driven RO and RRO osmotic desalination systems from water, energy, and environment relevance perspective: a comparative approach

Alireza Naminezhad[1] · **Mahmood Mehregan**[1]

Received: 25 August 2022 / Accepted: 12 December 2022 / Published online: 30 December 2022

Abstract
In this paper, two osmotic desalination systems, namely, plug reverse osmosis (RO) and recirculation reverse osmosis (RRO) systems integrated with solar and organic Rankine cycle (ORC), have been presented. These systems are modeled and optimized from energy, exergy, economic, and environmental perspectives. The objective functions are the concentration disposal index (CDI) and unit cost of the product (fresh water) (UPC). The results show that the RO cycle has an optimal configuration grounded on max (CDI) and min (UPC). At identical UPC, the environmental effects of the RO system were less than those of the RRO. This is attributed to higher recovery with increasing temperature of discharged water into the sea in a smaller area and at a higher rate. For the RO system, the values for CDI, exergy efficiency, and fresh water production are 0.193, 45.6%, and 13.1 m^3/h for R245ca fluid. Also, the share of RO and RRO in the total TAC costs is 19.44% and 17.33%, respectively. The R245ca working fluid is selected for both cycles, which is more productive than the other fluids. The results show that more than 50% recovery is achieved for the SW30HR-320 membrane at the optimum for the RO system.

Keywords Reverse osmosis (RO) · Solar energy · Organic Rankine cycle (ORC) · Recirculation RO (RO) · Environmental analysis · Water-energy-environment relevance

Introduction

Various technologies have been employed to produce fresh water, of which approximately 65% is pertinent to reverse osmosis (RO) systems (Jones et al. 2019; Fang et al. 2021). A present concern for RO desalination systems is their energy supply and environmental impact. In other words, the relevance between water, energy, and environmental impacts has become a topic of interest in desalination systems (Quan et al. 2021; Li et al. 2020; Chen et al. 2022).

A comprehensive study by Pugsley et al. (Pugsley et al. 2016) identified the need for solar energy for each country with water stress based on a defined index. Each country was assigned a rank in which, based on it, countries that have a high potential to produce fresh water at a reasonable price of solar energy are determined. The results of this study are presented in Table 1 for several Middle Eastern countries. This ranking factor, denoted by R, is defined based on the following parameters:

1. The amount of water stress in the country
2. Access to saline water sources, seawater, brackish water, and wastewater
3. Annual solar radiation area
4. The demand for fresh water in the coming years
5. Weather conditions

On the other hand, in the Persian Gulf, the Red Sea, and the eastern Mediterranean region, an increase in water salinity and the repercussions of desalination have been reported (Khudair and Eraibi 2017; Missimer and Maliva 2018; Chenoweth and Al-Masri 2022; Shahabi et al. 2015; Intakes and Outfalls for Seawater Reverse-Osmosis Desalination Facilities 2015). To clarify, a desalination system that uses only solar energy cannot be considered without environmental effects. Depending on the geographical location of each desalination plant, there are different methods for wastewater

✉ Alireza Naminezhad
ali.nami1029@gmail.com

[1] Faculty of Mechanical Engineering, Shahrood University of Technology, Shahrood, Iran

Table 1 R index on the priority of Middle Eastern countries for using solar energy for fresh water production, based on defined indicators (Pugsley et al. 2016)

Country	R index range
Saudi Arabia	$R \geq 5$
Oman	$R \geq 5$
Qatar	$R \geq 5$
Bahrain	$R \geq 5$
UAE	$R \geq 5$
Iran	$0.3 \leq R \leq 0.4$

disposal (Ge et al. 2019; Lin et al. 2021; Yang et al. 2022). The standard approach is to release the effluent into the sea and oceans. Approximately 5 to 10 km of the shoreline is affected by desalination effluents, eliciting environmental issues in the region. The results show that a large volume of brine is produced in the Middle East and North Africa. The volume of effluent in these areas is higher than one million barrels per day. This includes Saudi Arabia and Qatar, which produce 72 million cubic meters of fresh water per day (Pugsley et al. 2016). Research on the environmental impact of desalination projects has witnessed attention, increasing by 92% from 2005 to date (Ihsanullah et al. 2021; Yang et al. 2018).

Few papers have addressed the effects of the environment on desalination systems as a mathematical function and its impact on other cycle parameters. To express the environmental effects of brine, Shayesteh et al. (Shayesteh et al. 2019) presented a concentration disposal index (CDI) and evaluated a RO desalination system with an organic Rankine cycle (ORC) using heat recovery from exhaust gases to produce fresh water. The study's results signposted that the environmental effects can be thoroughly investigated using the expressed index regarding brine volume, temperature, and concentration effects. Also, optimizing the objective function positively influenced other cycle indicators, namely, exergy efficiency and water cost.

Mansouri et al. (Tajik Mansouri et al. 2019) integrated an RO desalination system with ORC and membrane desalination (MD) in an industrial unit. Using the CDI, the role of MD on the discharge brine from the RO system was investigated. The results of this study demonstrated that the arrangement of the ORC-RO-MD has a substantial role in reducing environmental effects but intensifies the overall cost of fresh water. In another study, Mansouri et al. (Tajik Mansouri et al. 2020) assessed the environmental effects of assorted ORC configurations using different fluids and the integration with RO-MD units, which utilized gas turbine exhaust. They studied approaches toward capturing CO_2 with algae and increasing fresh water production. The paper described the use of MD to reduce the RO environmental impact.

The configuration of the ORC-RO cycle whereby the output power of the ORC is set as the mover of the high-pressure pump has been studied in several articles. Table 2 delineates the research conducted on the mover supply of the RO system pump from different heat sources. As observed, the findings indicate that the optimization of this cycle and 4E analysis and environmental impacts have received less attention.

Limited research can be found comparing the two RO configurations. There are various configurations of the RO system, the two most common being Plug RO and recirculation RO (RRO). Khanarmuei et al. (Khanarmuei et al. 2017) compared these two configurations. The results of their study, which was performed for a fixed fresh water flow, exposed that in the optimal case, the RRO system reduced investment costs by 2% and increased maintenance costs by 6%, augmenting the efficiency by 19.7%.

In retrospect studies, only the ORC + RO system with heat recovery from an environmental perspective and 4E analysis was studied and analyzed. Fewer research works have focused on the present study innovations, namely:

(1) Analysis of Plug RO and RRO configurations from the perspective of 4E.
(2) Comparison of Solar + ORC + RO cycle configuration from the 4E perspective in tandem with its environmental effects.
(3) Using the environmental index to compare the two RO configurations and optimization through genetic algorithm (GA).
(4) Investigation and analysis of reducing the environmental effects of carbon dioxide production and energy availability for remote coastal areas with solar energy

Also, in this study, attributable to the increase in areas where desalination projects have led to an increment in seawater concentration, the environmental index along with energy, exergy, and economic analysis for the two configurations of the Solar + ORC + (RO/RRO) system is implemented.

System description

The studied cycle is illustrated in Fig. 1. Figure 1a shows the general structure of the cycle.

The cycle comprises three sections: solar farm, power generation, and fresh water production via RO. The parabolic solar field absorbs solar energy; the heat transfer fluid (HTF) enters the heat exchanger and absorbs heat, so its temperature is augmented. The heat exchanger has two parts, the economizer and the evaporator. The HTF leaves the heat exchanger by transferring heat to the organic working fluid and then enters the solar field through increased pressure. The solar field has different rings that are parallel to each

Table 2 Research on movers of RO system pumps from different heat sources

Authors	Heat source	Price of produced water ($/m^3)	Recovery (%)	Analysis*	Objective function
Shayesteh et al. (Shayesteh et al. 2019)	Solar	NA	18–21	2E	–
Tajik Mansouri et al. (Tajik Mansouri et al. 2019)	Solar	NA	–	1E	–
Tajik Mansouri et al. (Tajik Mansouri et al. 2020)	Solar	NA	–	1E	–
Manolakosa et al. (Manolakos et al. 2005)	Solar	–	–	1E	–
Delgado-Torres et al. (Delgado-Torres and García-Rodríguez 2007a)	Solar	–	18–21	1E	–
Delgado-Torres et al. (Delgado-Torres and García-Rodríguez 2007b)	Solar	2.03–14.85	50–75	2E	–
Delgado-Torres et al. (García-Rodríguez and Delgado-Torres 2007)	Solar	–	18–21	1E	–
Manolakosa et al. (Manolakos et al. 2007)	Solar	–	18–21	1E	–
Bruno et al. (Bruno et al. 2008)	Solar	–	18	1E	–
Manolakosa et al. (Manolakos et al. 2008)	Solar	6.85	–	2E	–
Manolakosa et al. (Manolakos et al. 2009a)	Solar	–	18	1E	–
Manolakosa et al. (Manolakos et al. 2009b)	Solar	6	–	2E	–
Kosmadakis et al. (Kosmadakis et al. 2009a)	Solar	–	–	1E	–
Kosmadakis et al. (Kosmadakis et al. 2009b)	Solar	0.68–0.9	–	2E	Cost of fresh water
Kosmadakis et al. (Kosmadakis et al. 2010a)	Solar	–		1E	–
Tchanche et al. (Tchanche et al. 2010)	Solar	–	15	1E	–
Nafey et al. (Nafey et al. 2010)	Solar	–	–	1E	–
Kosmadakis et al. (Kosmadakis et al. 2010b)	Solar	–	40	1E	–
Karellas et al. (Karellas et al. 2011)	Solar	–	50	1E	–
Delgado-Torresa et al. (Delgado-Torres and García-Rodríguez 2012)	Low-temperature heat source		50	2E	–
Peñate et al. (Peñate and García-Rodríguez 2012)	Geothermal	–	50	2E	–
Li et al. (Li et al. 2013a)	Solar	0.56	75	3E	Cost, recovery
Li et al. (Li et al. 2013b)	Heat recovery	–	30	3E	Efficiency cost, exergy
Geng et al. (Geng et al. 2016)	Heat recovery	–	–	2E	–
Mokhtari et al. (Mokhtari et al. 2016)	Solar	–	–	2E	–
Nemati et al. (Nemati et al. 2017)	Heat recovery	0.56	30	4E	Exergy efficiency, environmental impact, and cost
Igobo et al. (Igobo and Davies 2018)	Heat recovery	1.1	42	3E	Environmental and cost
Arab Chadegania et al. (Chadegani et al. 2018)	Heat recovery	NA	NA	3E	Annual profit and CO2 index
Izadpanah et al. (Izadpanah et al. 2022)	Heat recovery	0.53	46.14	4E	Makeup, UPC
JaliliJamshidian et al. (JaliliJamshidian et al. 2022)	Solar	2.08	50	2E	–
Jaafari and Rahimi (Jaafari and Rahimi 2021)	Heat recovery	2.84	39.24	4E	Exergy efficiency, UPC
Hassan et al. (Hassan et al. 2022)	Solar	–	–	4E	–

*1E: Energy, 2E: Exergy, Economic, 3E: Energy, Exergy, Economic, 4E: Energy, Exergy, Economic, Environmental impact

other. In other words, the HTF enters different branches, and each branch increases its temperature. The HTF experiences a pressure drop, which is compensated by the pump.

The organic fluid generates power in a simple organic Rankine cycle (ORC). At point (3), the organic fluid enters the tubing as saturation and produces power. Depending on its type, the organic fluid enters the condenser, either saturated or superheated as point (4) and condenses with a loss of energy to point (1). The organic fluid enters the pump, and its pressure increases as point (2) and exits the heat exchanger as condensed by passing through two heat exchangers. The contrast between the ORC system and the RO is observed at two points:

(1) The output power in the ORC is entirely given to the high-pressure pump of the RO system.
(2) Part of the water leaving the condenser enters the high-pressure pump.

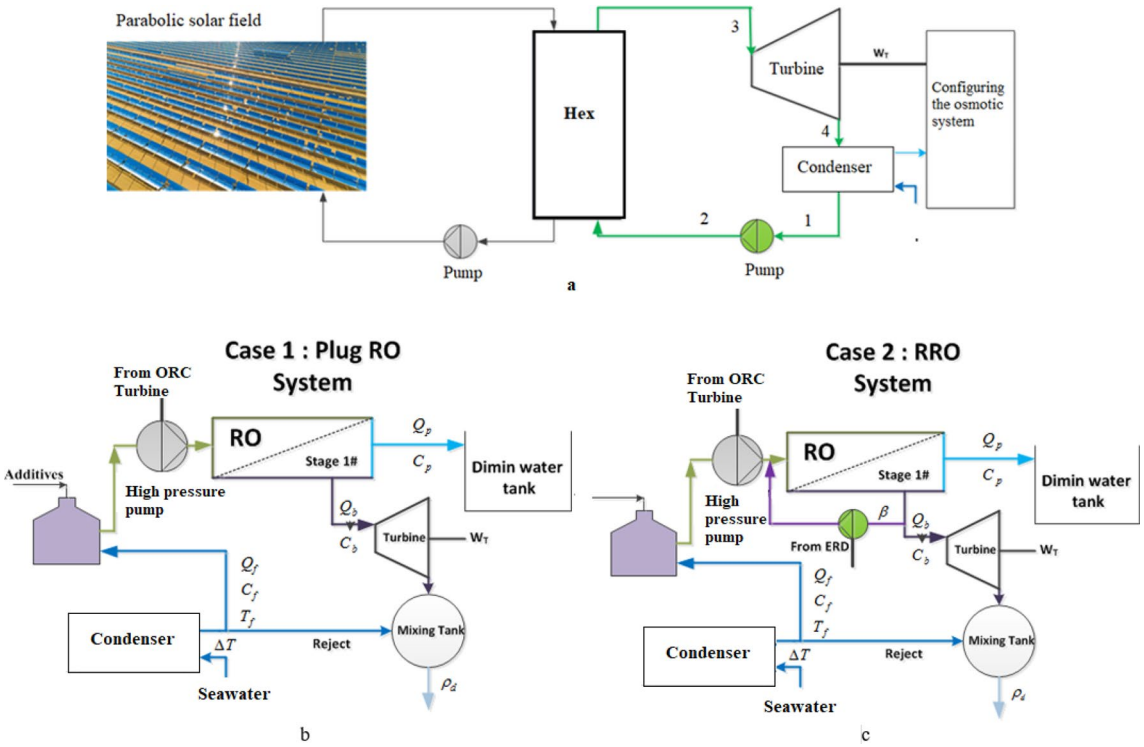

Fig. 1 Schematic of the studied system **a** general cycle configuration, **b** Plug RO system, **c** RRO system

In other words, the amount of heat rejected from the condenser increases the temperature of the water entering the osmotic system. In this section, both configurations for the osmotic system are suggested. The first configuration is the RO system that enters all the incoming water into the membranes, and the feed water is extracted as brine water and fresh water, as shown in Fig. 1b.

The second system is the RRO which enters a part of the brine water (β) due to the pressure and also the reduction of operation costs (power consumption) into the membrane section, depicted in Fig. 1c. After receiving heat, part of the seawater enters a mixed tank, and the other enters a tank, whereby additives such as sulfuric acid are added to adjust the pH. The output water from this tank enters a pump, whereby its energy is provisioned from the ORC cycle. The feed water is then divided into two streams of fresh and brine water. The difference between RO and RRO systems is in how brine water is used. An energy recovery system is designed for both cases.

What is important in this study is that the system's environmental effects are only in the output brine water. The solar part has no environmental effects. In the ORC, only the environmental effects, namely, ozone depletion potential (ODP) and global warming potential (GWP), should be considered in the working fluid selection. As a result, the most important part of the environmental impact of the studied body is the osmotic system.

Methodology

The nexus between energy, water production, and environmental effects in the proposed system is to increase power and fresh water production, respectively, with a decrease in environmental impacts. For this purpose, the two RO and RRO systems are compared from the 4E perspective in the optimal state. According to Fig. 2, the effect of each of the parameters of each part of the configuration is illustrated in each of the analyses. The effective parameters in energy and exergy analyses are similar, so they are expressed similarly. Some parameters affect only one item, and some affect most analyses.

This study aims to find the optimal expressed parameters so that the system has the lowest cost of fresh water production and the most negligible environmental impact. It can be seen that all parameters in the economic section are directly and indirectly affected. The final product of the fresh water production system, whereby increasing its production, improves the system's recovery and energy and exergy efficiency. In this optimization, the two osmotic configurations are compared based on the specified objectives to determine which systems can place the objective functions at their maxima.

In the RRO system, a percentage of brine (β) is returned to the system. It enters the membranes as feed water after passing through a booster pump, eliciting energy recovery.

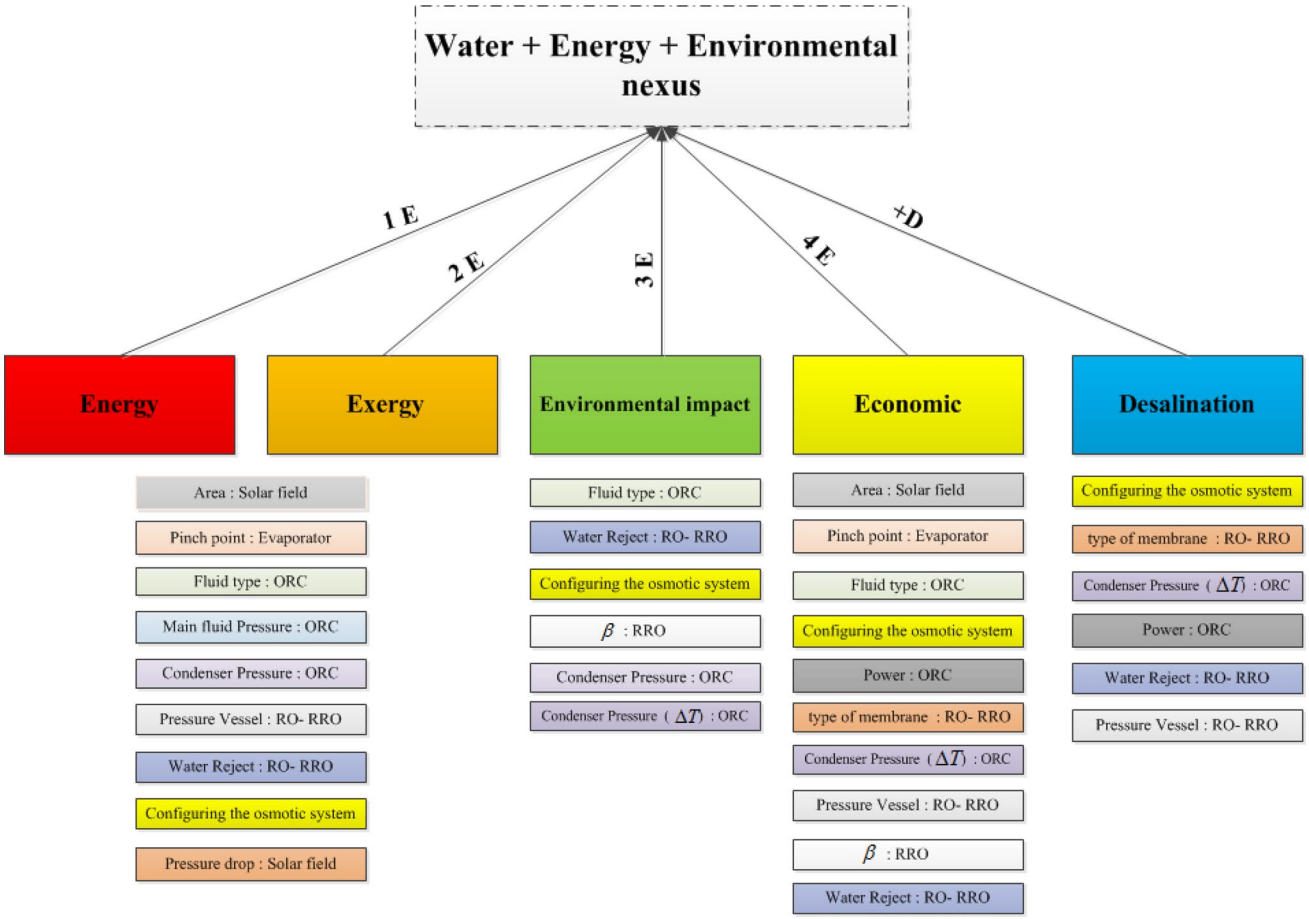

Fig. 2 Process block diagram

Adding some brine to the feed water increases the concentration, which causes more sedimentation, reducing the system's life. Through this approach, less brine is discharged into the environment. For this purpose, the two RO and RRO systems are optimized with identical parameters and ranges. This optimization is grounded on the two objective functions: CDI and prod. The two systems are compared at the optimal point found in the Pareto curve. Comparison under optimal conditions is instrumental in presenting a suitable configuration based on analysis of energy, exergy, economic, and environmental impacts along with fresh water production (4E + D) and optimal parameters.

Energy analysis (1E)

ORC

The fundamental equations used for the ORC system are based on the law of continuity and the first law of thermodynamics. The equations for the equipment used in the ORC cycle can be expressed as follows. In the turbine, based on the pressure, the saturation temperature and enthalpy of point (3) are determined according to the isentropic efficiency of the turbine ($\eta_T = 80\%$). According to Eq. (1), h_4 is determined, and according to the first law, the power capacity of the turbine ($\dot{W}_T$) is (Shayesteh et al. 2019):

$$\eta_T = \frac{h_3 - h_4}{h_3 - h_{4,is}} \tag{1}$$

$$\dot{W}_T = \dot{m}_3\left(h_3 - h_4\right) \tag{2}$$

In the condenser, the seawater exits the condenser with the determined temperature difference ($T_{cw,out} = T_{cw,in} + \Delta T$). By having the temperature of the inlet and outlet cooling water and the quality of the organic fluid and the condenser pressure at point (1) ($x = 0.0$ and P_{con}), the rejection heat and the amount of seawater can be calculated:

$$\dot{Q}_{cond} = \dot{m}_1\left(h_4 - h_1\right) \tag{3}$$

$$\dot{m}_{\text{water}} = \frac{\dot{Q}_{\text{cond}}}{Cp_{\text{water}}\Delta T} \tag{4}$$

In the pump, by determining the isentropic efficiency of the pump ($\eta_P = 85\%$), inlet, and outlet pressure, the power per unit mass is calculable. By calculating this value, the output enthalpy is also calculated:

$$W_p = \frac{(P_2 - P_1)}{\eta_P \rho_1} \tag{5}$$

$$h_2 = h_1 + W_p \tag{6}$$

Once the output enthalpy is determined, the required pump power can be calculated according to the first law of thermodynamics:

$$W_{p,1} = \dot{m}_1 (h_2 - h_1) \tag{7}$$

In the heat exchanger, the approach and pinch point temperature are determined as two parameters to find the temperature of the HTF entering and exiting the evaporator:

$$T_{\text{app}} = T_{\text{sat}} - T_{f,o,\text{Eco}} \tag{8}$$

$$T_{p.p} = T_{\text{HTF,out,Eva}} - T_{\text{sat}} \tag{9}$$

Next, according to the first law of thermodynamics, the inlet temperature of the HTF from the economizer ($T_{\text{HTF},i,\text{Eco}}$) and the flow rate of organic fluid ($\dot{m}_f$) as saturated are determined (Shayesteh et al. 2019):

$$\dot{m}_{\text{HTF}} Cp_{\text{HTF}} (T_{\text{HTF},o,\text{Eco}} - T_{\text{HTF},i,\text{Eco}}) = \dot{m}_f (h_{f,o,\text{Eco}} - h_{f,i,\text{Eco}}) \tag{10}$$

$$\dot{m}_{HTF} Cp_{HTF} (T_{HTF,o,Eva} - T_{HTF,i,Eva}) = \dot{m}_f (h_g - h_{f,o}) \tag{11}$$

RO and RRO

The design and modeling of the plug RO and RRO are similar. Only part of the brine flow rate is transferred to the inlet in the RRO system, which is determined by the feed water flow rate (Q_f) and the feed water concentration (C_f) according to the law of water-salt continuity. The RRO system generally reduces the number of elements to reach a fixed recovery but increases the operating costs and equipment required in the system. In modeling the osmotic system, the flowchart in Fig. 3 is employed. The feedwater flow rate is divided into several pressure pipes. The flow of feedwater enters the membrane, and each membrane is elementalized, and the fundamental equations described in the following are solved. This solution is repeated for the number of membranes in each pressure vessel (PV). Finally, the fresh water flow rate produced by each PV is summed, and the total fresh water flow rate is determined.

The basic equations for each element are as follows. The water flow flux is proportional to the feed water pressure (P_f), the required fresh water pressure (P_p), the osmotic pressure difference ($\pi_w - \pi_p$), and the membrane permeability (A) (Mokhtari et al. 2016; Khanarmuei et al. 2017):

$$J_w = A \times \text{TCF} \left[\left(P_f - P_p - \frac{\Delta P_f}{2} \right) - (\pi_w - \pi_p) \right] \times 10^6 \tag{12}$$

The amount of salt flow through the membrane is Eq. (13).

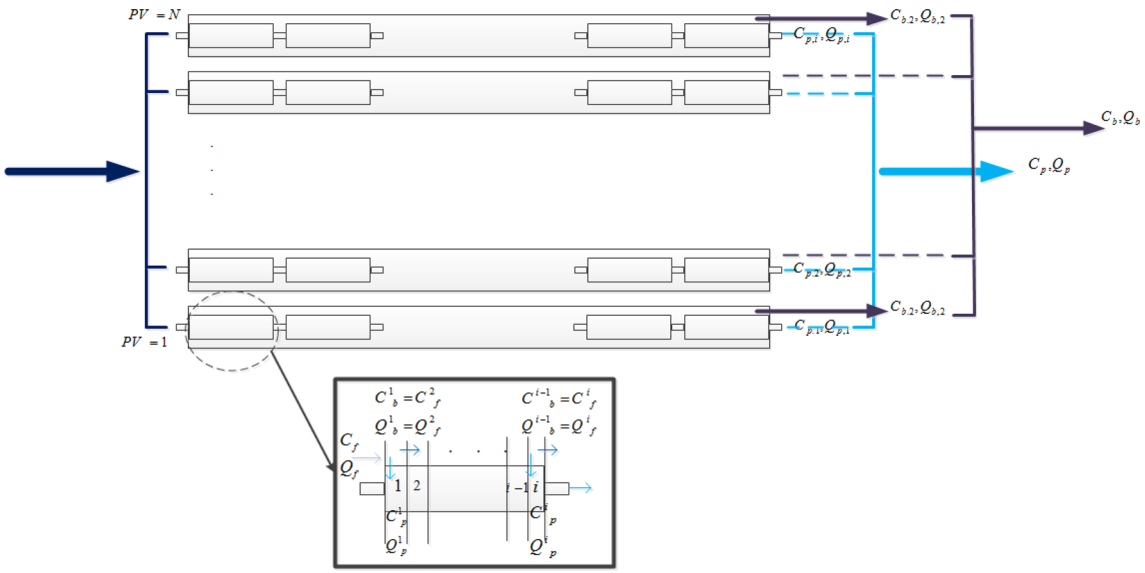

Fig. 3 The schematic of the osmosis system

$$J_s = B\left(C_w - C_f\right) \tag{13}$$

The flow rate is proportional to the difference between the wall concentration (C_w) and the salt concentration (C_f) (Mokhtari et al. 2016; Khanarmuei et al. 2017). The water velocity between the membranes is determined by Mokhtari et al. (2016); Khanarmuei et al. 2017):

$$V_w = \frac{J_s + J_w}{\rho_p} \tag{14}$$

Based on boundary conditions and polarization, the concentration on the wall is calculated as (Mokhtari et al. 2016; Khanarmuei et al. 2017):

$$C_w = C_p + \left(\frac{C_f + C_b}{2} - C_p\right) e^{\frac{V_w}{k}} \tag{15}$$

The concentration of fresh water produced and the fresh water flow rate is determined based on the following equations (Mokhtari et al. 2016; Khanarmuei et al. 2017):

$$C_p = \frac{J_s}{V_w} \times 1000 \tag{16}$$

$$Q_p = V_w S_m \tag{17}$$

The equations of salt and water continuity to determine brine concentration and flow rate are as follows:

$$C_B = \frac{Q_F C_F - Q_P C_P}{Q_B} \tag{18}$$

$$Q_B = Q_F - Q_P \tag{19}$$

The correction factor of temperature suggested for membranes of DOW is given as (Mokhtari et al. 2016; Khanarmuei et al. 2017):

$$\mathrm{TCF} = \begin{cases} \mathrm{EXP}\left[2640\left(\frac{1}{298} - \frac{1}{273+T}\right)\right], T \geq 25^{\circ}\mathrm{C} \\ \mathrm{EXP}\left[3020\left(\frac{1}{298} - \frac{1}{273+T}\right)\right], T \leq 25^{\circ}\mathrm{C} \end{cases} \tag{20}$$

The relationships between pressure drop and mass transfer have been determined by the Hagen–Poiseuille relationship and the Sherwood and Schmidt numbers, consistent with references (Mokhtari et al. 2016; Khanarmuei et al. 2017).

Due to the range of discharge and insignificant changes in efficiency, its value is chosen as 90% in this modeling.

Parabolic solar farm

In this model, each tube is elementalized, and the HTF absorbs the irradiation energy from the sun in the tubes, while part of it is lost through the surrounding environment. The flow rate from each branch of the farm is calculated according to the law of continuity ($\dot{m}_{pip} = \rho_{oil} V A_{pipe}$). The energy absorbed by the HTF is calculated as (Mokhtari et al. 2016):

$$\dot{q}_{abs} = h_i D_{in} \pi \left(T_m - T_{f,ave}\right) \tag{21}$$

$$h_i = Nu_{D_{in}} \frac{k}{D_{in}} \tag{22}$$

$$\dot{q}_{abs} = \dot{m}_{pip} Cp_{HTF} \left(T_{f,out} - T_{f,in}\right) \tag{23}$$

Based on Eq. (23), the temperature of the HTF outlet from each element can be calculated. The Nusselt number in laminal and turbulent flows can be calculated. To determine the Nusselt number for turbulent flow, Eq. (24) is employed (Mokhtari et al. 2014):

$$\mathrm{Nu}_{D_2} = \frac{\frac{f}{8}(\mathrm{Re} - 1000)\,\mathrm{Pr}}{1 + 12.7\sqrt{\frac{f}{8}}\left(\mathrm{Pr}^{\frac{2}{3}} - 1\right)} \tag{24}$$

$$f = \left(1.82 \log\left(\mathrm{Re}_{D_{\mathrm{in}}}\right) - 1.64\right)^{-2} \tag{25}$$

where f is the coefficient of friction for the inner surface of the absorbent tube and Pr is the Prandtl number for the operating fluid, respectively. When the flow is laminar, the Reynolds number has a constant value. Heat transfer from the surface of the absorbent tube to the environment occurs through both convection and radiation, determined as follows:

$$q_{\mathrm{loss}} = h_o \pi D_{\mathrm{out}} \left(T_m - T_{\mathrm{amb}}\right) \tag{26}$$

$$h_o = \frac{k}{D_{\mathrm{out}}} \mathrm{Nu}_{D_{\mathrm{out}}} \tag{27}$$

As previously described, convective heat transfer is calculated from Newton's law of cooling, and only the Nusselt numbers change due to changing conditions. To calculate the Nusselt in the case where there is no wind, the equations proposed by Churchill and Chu are employed, and in the present modeling, this case is assumed (Mokhtari et al. 2016):

$$\mathrm{Nu}_{D_{\mathrm{out}}} = \left\{0.06 + \frac{0.387 Ra_{D_{\mathrm{out}}}^{1/6}}{\left[1 + (0.559/\mathrm{Pr})^{9/16}\right]^{8/27}}\right\}^2 \tag{28}$$

$$\mathrm{Ra}_{D_{\mathrm{out}}} = \frac{g\beta\left(T_w - T_{\mathrm{amb}}\right)D_{\mathrm{Out}}^3}{(\alpha\nu)} \tag{29}$$

$$\beta = \frac{1}{T_{\mathrm{ave}}} \tag{30}$$

where Ra, β, ν, and Pr are Rayleigh number, the coefficient of volumetric thermal expansion, the kinematic viscosity, and Prandtl number at the average ambient and tube temperature, and T_{ave} is the average surface and ambient temperature.

Exergy analysis (2E)

Exergy of any stream includes physical and chemical exergy as described in Bejan et al. (1995):

$$\dot{E}x = \dot{E}x^{\mathrm{PH}} + \dot{E}x^{\mathrm{CH}} \tag{31}$$

Based on different fluids, exergy is expressed in Table 3, and the specific exergy power is determined. Due to the fact that the salt concentration changes in the fresh water production process, the amount of chemical exergy is calculated based on Ref. (Bejan et al. 1995).

After calculating the exergy of each stream, the amount of exergy destruction ($\dot{E}x_D$) is calculated as (Bejan et al. 1995):

$$\dot{E}x_Q + \sum_i \dot{m}_i ex_i = \sum_e \dot{m}_e ex_e + \dot{E}x_W + \dot{E}x_D \tag{32}$$

In this equation, $\dot{E}x_Q$ and $\dot{E}x_W$, respectively, denote the exergy of the transferred heat and the work done. The parameters expressed in this regard are determined as follows (Bejan et al. 1995):

$$\dot{E}x_D = T_0\dot{S}_{\mathrm{gen}} \tag{33}$$

$$\dot{E}x_Q = \int_i^e \left(1 - \frac{T_0}{T_b}\right)q'\,\mathrm{d}L \tag{34}$$

$$\dot{E}x_W = \dot{W} - p_0\frac{\mathrm{d}V_{cv}}{\mathrm{d}t} \tag{35}$$

Based on Ref. (Bejan et al. 1995), the exergy balance for each stream can be expressed as follows:

$$\dot{E}x_f = \dot{E}x_P + \dot{E}x_D + \dot{E}x_L \tag{36}$$

where $\dot{E}x_f$, $\dot{E}x_P$, and $\dot{E}x_L$ express fuel exergy, product exergy, and lossed exergy, respectively. Based on this definition, the exergy efficiency can be defined as follows:

$$\eta_{ex} = \frac{\dot{E}x_p}{\dot{E}x_{f,\mathrm{int,Plant}}} \xrightarrow{Eq(15)} = 1 - \frac{\dot{E}x_D + \dot{E}x_L}{\dot{E}x_{f,\mathrm{int,Plant}}} \tag{37}$$

Exergy equations for equipment in the cycle are charted in Table 4.

Economic analysis (3E)

In this section, economic analysis has been considered. The total annualized cost (TAC) consists of two terms: total capital cost (TCI) and operating cost (OC). TCI includes fixed-capital investment (FCI), start-up cost (SUC), working capital (WC), allowance for funds of construction (AFUDC) and licensing, research, and development (LRD) costs (Khanarmuei et al. 2017; Bejan et al. 1995):

$$\mathrm{TCI} = \mathrm{FCI} + \mathrm{SUC} + \mathrm{WC} + \mathrm{LRD} + \mathrm{AFUDC} \tag{38}$$

The direct cost (DC) is determined by Eq. (39), which contains the onsite (ONSC) and (OFSC) offsite costs (Bejan et al. 1995):

$$\mathrm{DC} = \mathrm{ONSC} + \mathrm{OFSC} \tag{39}$$

$$\mathrm{OFSC} = \begin{cases} 1.2 \times \mathrm{ONSC} & \text{new system} \\ 0.45 \times \mathrm{ONSC} & \text{expansion} \end{cases} \tag{40}$$

Assuming that R&D costs are calculated as follows:

$$\mathrm{LRD} = \mathrm{AFUDC} + 0.15 \times \mathrm{FCI} \tag{41}$$

In this case, the TCI can be calculated through:

$$\mathrm{TCL} = 147 \times \mathrm{FCI} \tag{42}$$

As a result:

Table 3 Chemical and physical exergies in each section (Tajik Mansouri et al. 2020; Bejan et al. 1995)

Section	Physical exergy	Chemical exergy
Power production	$ex^{ph} = (h - h_\circ) - T_\circ(s - s_\circ)$	$ex^{ch} = m_i ex_s^{ch_i}$
Fresh water production		$ex_{sw}^{ch} = \sum_{i=1}^{n} w_i\left(\mu_i - \mu_0\right)$
		$\mu_w = \frac{\partial G_{sw}}{\partial m_w} = g_w - w_s\frac{\partial g_{sw}}{\partial w_w}$
		$g_{sw} = h_{sw} - (T - 273.15)s_{sw}$
		$\frac{\partial g_{sw}}{\partial w_s} = \frac{\partial h_{sw}}{\partial w_s} - (T - 273.15)\frac{\partial s}{\partial w_s}$

Table 4 Exergy balance equations and functions for equipment

Component	Exergy equation
Turbine	$E\dot{x}_D = E\dot{x}_3 - E\dot{x}_4 - \dot{W}_T$ $E\dot{x}_F = E\dot{x}_3 - E\dot{x}_4$ $E\dot{x}_P = \dot{W}_T$ $\eta_{Ex} = \frac{E\dot{x}_P}{E\dot{x}_F} \rightarrow \eta_{Ex} = \frac{\dot{W}_T}{E\dot{x}_3 - E\dot{x}_4}$
Pump	$E\dot{x}_D = \left(\dot{W}_P + E\dot{x}_1\right) - E\dot{x}_2$ $E\dot{x}_F = \dot{W}_P$ $E\dot{x}_P = E\dot{x}_2 - E\dot{x}_1$ $\eta_{Ex} = \frac{E\dot{x}_2 - E\dot{x}_1}{\dot{W}_P}$
Solar	$E\dot{x}_D = \left(\dot{W}_P + E\dot{x}_{Solar}\right) - \left(E\dot{x}_{out,HEX} - E\dot{x}_{in,HEX}\right)$ $E\dot{x}_F = \dot{W}_P + E\dot{x}_{Solar}$ $E\dot{x}_P = E\dot{x}_{out,HEX} - E\dot{x}_{in,HEX}$ $\eta_{Ex} = \frac{Ex_D}{\dot{W}_P + E\dot{x}_{Solar}}$
Condenser	$E\dot{x}_D = \left(E\dot{x}_4 + E\dot{x}_{waterin}\right) - \left(E\dot{x}_1 + Ex_{Waterout}\right)$ $E\dot{x}_F = E\dot{x}_{waterin} - Ex_{Waterout}$ $E\dot{x}_P = E\dot{x}_4 - E\dot{x}_1$ $\eta_{Ex} = \frac{E\dot{x}_4 - E\dot{x}_1}{E\dot{x}_{waterin} - E\dot{x}_{Waterout}}$
HEX	$E\dot{x}_D = \left(E\dot{x}_{Oil,in} + E\dot{x}_6\right) - \left(E\dot{x}_{Oil,out} + E\dot{x}_5\right) E\dot{x}_F = E\dot{x}_{Oil,in} - E\dot{x}_{Oil,out}$ $E\dot{x}_P = E\dot{x}_3 - E\dot{x}_2$ $\eta_{Ex} = \frac{E\dot{x}_3 - E\dot{x}_2}{E\dot{x}_{Oil,in} - E\dot{x}_{Oil,out}}$
RO, RRO	$E\dot{x}_D = \dot{W}_{rev(\max)} - \dot{W}_{Pump}$ $E\dot{x}_F = \dot{W}_{pump}$ $\eta_{Ex} = \frac{E\dot{x}_D}{E\dot{x}_F}$

$$\mathrm{TCL} = 1.184\mathrm{DC} = 1.84 \times (\mathrm{ONSC} + \mathrm{OFSC}) \tag{43}$$

TCI can also be determined by combining the above relations:

$$\mathrm{TCI} = \begin{cases} 4.05\ \mathrm{ONSC} & \text{new system} \\ 2.67\ \mathrm{ONSC} & \text{expansion} \end{cases} \tag{44}$$

According to the cost of purchasing equipment (CC) or ONSC, the TCI can be evaluated. The relations for estimating the cost of each element of the osmosis system, the ORC, and the parabolic solar farm, along with other costs of available equipment such as steam turbines and condensers, are shown in Table 5.

The operating cost of a reverse osmosis system is calculated as follows, and in other systems, 2% of the CC is considered as O&M costs (Nabati and M.S. sadeghi, S.N. Naserabad, H. Mokhtari, S. izadpanah 2018).

$$\mathrm{OC}_m = 0.2\mathrm{CC}_m \tag{45}$$

$$\mathrm{OC}_{\mathrm{ins}} = 0.005 \times \mathrm{TCI} \tag{46}$$

$$\mathrm{OC}_{\mathrm{lab}} = Q_p \times 24 \times 365 \times f_c \times 0.01 \tag{47}$$

$$\mathrm{OC}_{\mathrm{ch}} = Q_p \times 24 \times 365 \times f_c \times 0.0225 \tag{48}$$

$$\mathrm{OC}_{\mathrm{main}} = Q_p \times 24 \times 365 \times f_c \times 0.01 \tag{49}$$

$$\mathrm{OC}_{O\&M,\mathrm{RO}} = \mathrm{OC}_{\mathrm{ins}} + \mathrm{OC}_{\mathrm{labor}} + \mathrm{OC}_{\mathrm{ch}} + \mathrm{OC}_{\mathrm{main}} \tag{50}$$

where OC_m is the replacement cost; $OC_{O\&M}$ is the total operating cost, which includes OC_{lab}, OC_m, OC_{ins}, and OC_{ch} which are the annual cost of the labor, maintenance, insurance, and chemicals, respectively. The operating costs of other components have also been calculated according to Ref. (Bejan et al. 1995). Finally, the annual operating cost is calculated as follows:

$$\mathrm{AOC}_{\mathrm{RO}} = \mathrm{OC}_m + \mathrm{OC}_{O\&M,\mathrm{RO}} \tag{51}$$

$$\mathrm{AOC}_{\mathrm{Total}} = \mathrm{AOC}_{\mathrm{Other}} + \mathrm{AOC}_{\mathrm{RO}} \tag{52}$$

The normalized TAC is given as:

$$\mathrm{TAC} = \frac{\mathrm{TCI}}{\mathrm{CRF}} + \mathrm{AOC}_{\mathrm{Total}} \tag{53}$$

where CRF is the capital recovery factor. Finally, the unit product cost (UPC) of fresh water is defined as:

$$\mathrm{UPC} = \frac{\mathrm{TAC}}{24 \times Q_p \times 365} \tag{54}$$

Environmental effects (4E)

In this study, the organic fluids charted in Table 6, which have appropriate environmental conditions suggested by ASHRE, are considered in the modeling.

RO system

In this study, the environmental impact function of brine is carried out similar to Refs. (Shayesteh et al. 2019; Tajik Mansouri et al. 2020):

$$\mathrm{CDI} = R\rho_\alpha \rightarrow \text{Where } \rho_\alpha = \frac{\rho_{sw} - \rho^*_{1,d}}{\rho^*_{2,d} - \rho_{sw}} \begin{cases} \rho_{sw} = f\left(C_{sw}, T_{sw}\right) \\ \rho^*_{1,d} = f\left(C_{sw}, T_d\right) \\ \rho^*_{2,d} = f\left(C_d, T_{sw}\right) \end{cases} \tag{55}$$

In this dimensionless function, recovery is a function that reduces with increasing flow rate. Owing to the slight effect of temperature on density at low temperatures for water, this function is based on the more it increases, the environmental effects lessen. On the other hand, density of brine depends on salinity. The salinity of seawater is considered as a basis because the brine water is discharged into the sea. Therefore, the difference between the density of brine water and seawater is considered at a constant temperature. The lower the amount,

Table 5 The equations for estimating the cost components

Component	Equation
Capital cost for the pre-treatment and seawater intake	$CC_{SWIP} = 996\left(Q_f 24\right)^{0.8}$
Capital cost for the pre-treatment and high-pressure pump	$CC_{hpp} = 52\left(Q_{hpp}\Delta P_f\right)$
Total membrane module cost	$CC_m = \sum_{j=1}^{N_{RO}} C_k n_{m,j} n_{PV,j} + \sum_{j=1}^{N_{RO}} C_{PV} n_{pv,j}$
Turbine	$CC_{Turbine} = 3880.5\dot{W}_T^{0.7}\phi_\eta\phi_T$ $\phi_\eta = \left(1 + \left(\frac{1-0.95}{1-\eta_T}\right)\right)^4$ $\phi_T = \left(1 + 5\left(\exp\left(\frac{T_3-866}{10.42}\right)\right)\right)$
Condenser	$CC_{cond} = \frac{280.74\dot{Q}_{cond}}{2200\Delta T} + 746\dot{m}_{water} + 70.5\dot{Q}_{cond}\times$ $\left(-0.6936\ln\left(T_{cw,out} - T_{cw,in}\right) + 2.1897\right)$
Pump	$\mathrm{CC}_p = 549.13\left(W_P\right)^{0.71} f_m \cdot \phi_\eta$ $\phi_\eta = 1 + \left(\frac{1-0.8}{1-\eta_1}\right)^3$ $\mathrm{f_m} = \begin{cases} castiron = 1 \\ Steel = 1.41 \end{cases}$ $\mathrm{f_m}$: correction factor of material,$\mathrm{f_m} = 1.41$
HEX	$CC_{WHR} = c\left[\left(\frac{\dot{Q}_{\mathrm{Eco}}}{LMTD_{Eco}}\right)^{0.8} + \left(\frac{\dot{Q}_{\mathrm{Eva}}}{LMTD_{\mathrm{Eva}}}\right)^{0.8}\right] +$ $d \times \dot{m}_{ORC} + e \times \dot{m}_{\mathrm{Gas}}^{1.2}$ $c = 6570\frac{\$}{(\mathrm{kW/K})^{0.8}}$ $d = 21276\frac{\$}{(\mathrm{kg/s})}$ $e = 1184.4\frac{\$}{(\mathrm{kg/s})^{1.2}}$
Solar field	355 $ per square meter
Pelton turbine	$\log_{10}\left(CC_{Pelton}\right) = 2.2476 + 1.4965\log_{10}\left(\dot{W}_{Pelton}\right) - 0.161\left(\log_{10}\left(\dot{W}_{Pelton}\right)\right)^2$

Table 6 Thermodynamic and environmental properties of organic working fluids (Tajik Mansouri et al. 2020)

No.	Fluid	GWP	ODP	ASHRAE Standard 34*
1	R141b	700	0.11	–
2	R11	4750	1	**A1**
3	R364mfc	890	–	–
4	R123	120	0.02	**B1**
5	R245ca	640	0	–
6	R1233zd	4.5	0,00,034	**A1**
7	R245fa	950	0	**B1**
8	R114	10,040	1	**A1**
9	R236ea	1200	0	–
10	R236fa	1030	0	**B1**

*Refrigerant safety classification 1: no flammability, 2: less flammability, 3: higher flammability, (A) less toxicity, (B) higher toxicity

Bold indicates level of flammability and toxicity of organic fluid

the less environmental impact it has on the sea. That is why it is located in the denominator.

Optimization

The two configurations are optimized separately based on optimization variables in Table 7.

Validation

For validation, the ROSA software has been used to validate the code developed in MATLAB software. In this validation for the plug system, the flow rate and feed water concentration are TDS 4049 and 40 m^3/h, respectively, and the results are presented in Table 8.

Table 7 Optimization results based on the best optimal point

Parameter	Upper boundary	Lower boundary	Unit	Note
Inlet pressure to the turbine	4200	700	kPa	Based on the critical fluid pressure
Condenser temperature	40	60	°C	The water temperature rises to 35 °C
Pinch-point temperature	10	150	°C	Outlet oil temperature limit from HEX
Approach temperature	5	10	°C	–
Recovery	10	55	%	Based on the recommendation of DOW
Number of membranes per PV	2	8	–	Based on the of DOW
Difference between the inlet and outlet water	5	10	°C	–
Percentage of rejected water	0	95	%	–
Percentage of water returned (β)	0	50	%	–
Absorbent diameter	29	80	mm	Construction of equipment
Pipe thickness	2	25	mm	–
Collector width	3.5	8	m	Construction of equipment
Speed inside pipe	1	2.2	m/s	Prevention of corrosion

Table 8 Validation results with ROSA software

Parameter	ROSA software results	Simulation results	Different (%)
Concentration of fresh water (ppm)	*23.5*	*21.93*	*7.1*
Fresh water production (m^3/h)	*30.83*	*30.12*	*1.7*
Pressure of inlet feed (MPa)	*3.77*	*3.52*	*6.6*
Recovery of water (%)	*75*	*75*	*0*

Italic values indicate the results of validation with the ROSA software and error percentage

Results and discussion

In multi objective optimization, it is required to define a process for the optimal solution among available solutions. In the literature many methods can be found in this regard. In many cases the dimensions of two or more objectives are different, so, firstly, dimensions and scales of the objectives should be unified. Therefore, objectives vectors should be non-dimensionalized before decision-making. There are some methods of non-dimensionalization utilized in decision-making including linear non-dimensionalization, Euclidian non-dimensionalization, and fuzzy non-dimensionalization, which have been comprehensively described in Sayyaadi and Mehrabipour (2012).

In the literature, several methods of decision-making processes, including the fuzzy Bellman-Zadeh, LINMAP, and TOPSIS, have been used in order to specify the final optimal solution. In this paper, LINMAP method has been employed for this purpose. LINMAP employs Euclidian non-dimensionalization, and after Euclidian non-dimensionalization of all objectives, the spatial distance of each solution on the

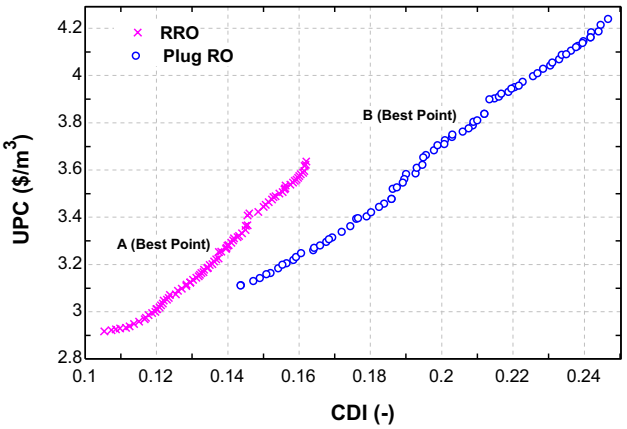

Fig. 4 Pareto curves obtained from RO and RRO system optimization

Pareto frontier from the ideal point denoted by d_{i+} is determined. For the determination of the ideal point, which is in the infeasible domain, the process ahead is passed. After the creation of the Pareto curve among the points found, the amounts of the (X_{ideal}, Y_{ideal}, Z_{ideal}) of the ideal point are chosen. For the objective functions which are considered to be maximized (like the CDI (Max (F_j)), the maximum amount and for the functions which are considered to be minimized (like UPC Min (F_j)), the minimum obtained amount is chosen. This obtained point is the ideal point with the maximum and minimum amount of the objective functions.

Figure 4 shows the optimization Pareto curve of the two systems cycles, RO and RRO, with two target functions of UPC and CDI. The goal of the optimization is to increase the CDI function and reduce the UPC. In the Pareto curves relevant to the CDI, the UPC of the RO system is higher than the RRO system. The Pareto curve divides the solution

region into two: the accessible and the inaccessible. The RO system Pareto curve is located in the inaccessible part of the RRO system, which signposts the appropriate optimal points of this system.

The optimization results based on the best optimal point are presented in Table 9. It is observed that in an almost constant TAC, the exergy efficiency for RO and RRO is 45.6% and 38.2%, respectively. The share of RO and RRO in the total TAC costs also shows that the RRO has 19.44% compared to RO, which has 17.33% poses more costs to the system. Also, the RRO has increased ancillary costs by 3.8%. This is due to the increase in costs, including increased sedimentation and replacement of membranes.

Moreover, due to the increase in input brine concentration and specific energy consumption (SEC), the RRO exergy efficiency is 26.6% lower than that of RO. Table 9 shows that the exergy efficiency of the whole cycle with RO is 40.68% and for the RRO is 38.2%. This is attributable to the production of more fresh water in exchange for less energy consumption. It is observed that to augment efficiency, the genetic algorithm has increased the pump pressure as much as possible, and its value has not exceeded 80 bar. Consistent with the membranes used, if the pressure increases from this value, there is the possibility of rupture and damage to the membrane. In the RRO system, since approximately 13.5% of the water is recirculated to it, this has reduced the pressure of the feed pump.

The fresh water flow rate produced in the RRO system is more than RO, which is because of the brine water injection into the feed water. A notable point is the change in the selection of membranes based on the input feed water. Based on the condition of the feed water, which has a concentration of 42,000 ppm (concentration of water in the Persian Gulf), the SW30HR-320 membrane is used for the RO system, which is a common membrane that has high strength in rejecting salts. But in the RRO system, SW30XLE-400i is employed because:

1. Operating cost for high TDS.

Table 9 Optimization results based on the best optimal point

Parameters	RO	RRO
Total annual cost ($/year)	36,964.90	36,066.25
TAC_{RO} (%)	17.13	19.44
AOC_{RO} ($/year)	2026.50	2107.60
RO/RRO exergy efficiency (%)	40.68	32.13
Total exergy efficiency (%)	45.6	38.2
Net power plant (kW)	84.39	91.87
Energy efficiency ORC (%)	10.73	13.08
Heat losses in condenser (kW)	786.49	702.37
Fresh water product (m^3/h)	13.1	14.2
The feed pressure (bars)	79.99	79.63
Concentration of permeate (ppm)	851.73	961.68
Specific energy consumption with ERD (kWh/m^3)	2.79	4.14
Specific energy consumption without ERD (kWh/m^3)	4.94	5.97
Recovery (%)	52.28	48.76
Total exergy destruction (kW)	735.84	720.15
Unit product cost ($/$m^3$)	3.59	3.22
Type of membrane	SW30HR-320	SW30XLE-400i
Concentration of brine (ppm)	95,471.91	94,699.30
Brine product (m^3/h)	4.29	5.05
Dilution of the concentrate (ppm)	60,499.02	67,622.19
Temp. of steam diluted Dilution of the concentrate (C)	36.31	37.69
Mass flow rate of diluted (m^3/h)	146.5	113.6
CDI	0.193	0.137
Working fluid (%)	R245ca	R245ca
Beta	–	13.49
The diameter of the absorbent tube	23.3	33.3
The thickness of the absorbent tube	3.3	3
Velocity inside pipe	2.3	1.7
The width of the collector	7.9	7.7

2. Due to its high surface area, it has a significant production of fresh water.
3. For systems with low recovery, it can cut the risk of clogging,

On the basis of all these issues existing in the RRO system, the genetic algorithm has selected this membrane. Figures 5 and 6 show the membrane sensitivity analysis in the RO system. As seen, the SW30HR-320 produces less fresh water than the SW30XLE-400i due to its lower membrane surface area (Fig. 5) but has a higher salt rejection (Fig. 6). Increasing the concentration and decreasing the flow rate is due to the polarization effect of the concentration on the surface, which momentously increases the salt concentration of the wall. Increasing water temperature and decreasing brine flow rate (increasing recovery) have caused the value of the CDI function in the RO system to be higher than the RRO system. As a result, it is discerned that a 10.5% increase in concentration has again improved the CDI function compared to the RRO system. In other words, environmental issues for the osmotic system must be addressed in an inclusive and comprehensive manner. Temperature, concentration, and water flow all affect this function. Since it is discharged to the sea floor, temperature term is the main factor in reducing the mixing time with seawater and reducing the area affected by the brine discharge. The subjection of bioavailability into the discharged water into the sea leads to a reduction in mixing time and a smaller area affected by this osmotic system due to the temperature difference.

In Figure 5, it can be seen that according to Eq. (15), with the increase of the input rate, the water concentration near the wall increases, and this increases the osmotic pressure in Eq. (12), which reduces the amount of water flux from the membrane.

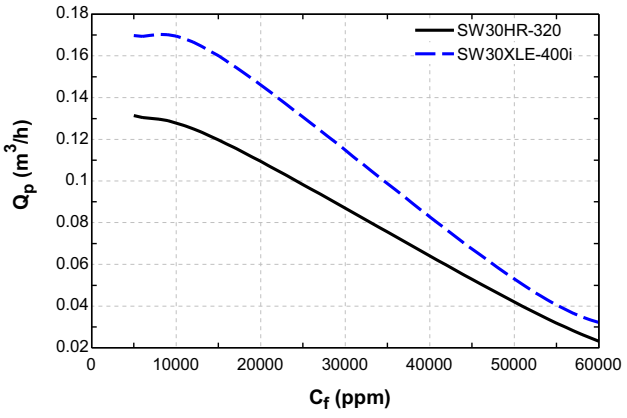

Fig. 5 Sensitivity analysis of produced fresh water flow rate on membrane change in different concentrations of inlet water on the membrane

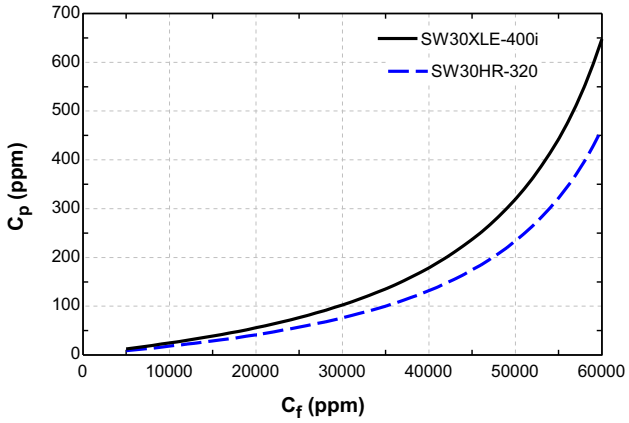

Fig. 6 Sensitivity analysis of produced fresh water concentration on membrane change at different concentrations of inlet water on a membrane

Figure 7 illustrates the effect of recovery with SW30HR-320 on SEC. It can be seen that the energy consumption for the SW30HR type membrane reaches its lowest level in the range of 50% water recovery. Therefore, it is better than the recovery be within this range in the design of systems that use this membrane. According to Table 9, it is conspicuous that the genetic algorithm based on the selected membrane has placed the system recovery in this range.

The reason for the decrease in SEC and then its increase is due to the flow rate and inlet pressure. As the recovery increases, the flow rate decreases, but the inlet pressure increases so that the recovery can be increased; this leads to SEC decreasing at first and then increasing.

Figure 8 depicts the sensitivity analysis on the different working fluids in the RO cycle. It is observed that the type of working fluid is very effective on the production capacity. By changing the type of fluid at a constant operating

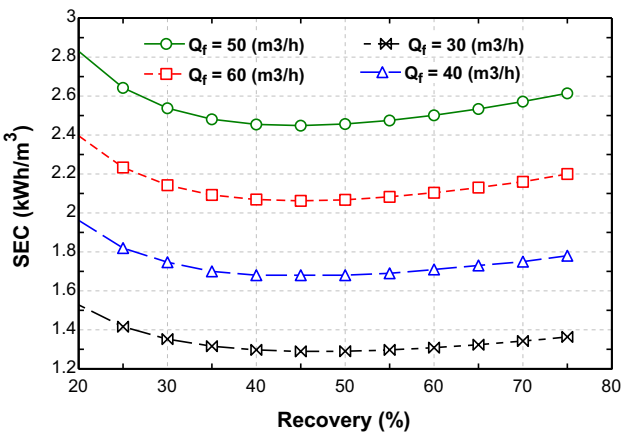

Fig. 7 The effect of recovery with SW30HR-320 on SEC in different flow rates

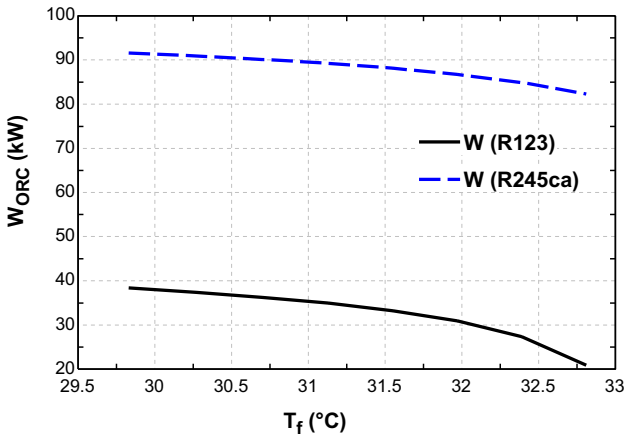

Fig. 8 The effect of inlet water temperature on output power in different working fluids

pressure, the enthalpy of stream to the turbine and the condenser pressure is altered. These two parameters influence the ORC turbine, leading to a variance in power produced. By changing the fluid R245ca to R123, it is demonstrated that the power is reduced by 55%. At high temperatures, the effect of condenser pressure can be considered as a factor of further reduction of turbine power. It should be noted that with decreasing power, the pump pressure of the RO system will also lessen, and fresh water production will decline.

Figure 8 is obtained by changing the fluid in thermodynamically stable conditions. This figure shows the working fluid analysis. By changing the fluid and not changing the thermodynamic conditions, it can be seen that the condenser pressure increases in the R123 fluid, and the input enthalpy to the turbine decreases; this leads to a reduction in power when the fluid is changed from R245ca to R123.

Conclusion

In this paper, the two solar-driven osmotic systems fed on seawater, namely, plug RO and RRO, were assessed and compared in terms of energy, exergy, economics, environmental impact, and fresh water production (4E + D). The purpose of this study was to compare the two cycles under optimal conditions to reduce fresh water costs and increase the environmental impact index. Since the solar field power generation cycle was combined with ORC, the only environmental effect of the system under consideration was the osmotic system. The genetic algorithm found optimal parameters by simulating the three sections: the parabolic solar field, the ORC cycle, and the osmotic RO and RRO systems. The results showed that the RO cycle has an optimal configuration grounded on the objective functions (max (CDI), min (UPC)). At identical UPC, the environmental effects of the RO system were less than those of the RRO. This was attributed to higher recovery with increasing temperature of discharged water into the sea, which took place in a smaller area and at a higher rate. The results indicated that the total system exergy efficiency for RO and RRO was 45.6% and 38.2%, respectively. Also, the share of RO and RRO in the total TAC costs was 19.44% and 17.33%, respectively. The R245ca working fluid was selected for both cycles, which is more productive than the other fluids. The sensitivity analysis results signposted that 50% recovery elicited in best SEC for the SW30HR-320 membrane, which the genetic recovery algorithm calculated it at 52% for the RO system.

Funding There is no funding.

Data availability There are no data for this paper.

Declarations

Conflict of interest The author declares no conflict of interest.

References

Bejan A, Tsatsaronis G, Moran MJ (1995) Thermal design and optimization. Wiley, Hoboken

Bruno JC, López-Villada J, Letelier E, Romera S, Coronas A (2008) Modelling and optimisation of solar organic rankine cycle engines for reverse osmosis desalination. Appl Therm Eng 28:2212–2226. https://doi.org/10.1016/j.applthermaleng.2007.12.022

Chadegani EA, Sharifishourabi M, Hajiarab F (2018) Comprehensive assessment of a multi-generation system integrated with a desalination system: modeling and analysing. Energy Convers Manag 174:20–32. https://doi.org/10.1016/j.enconman.2018.08.011

Chen F, Ma J, Zhu Y, Li X, Yu H, Sun Y (2022) Biodegradation performance and anti-fouling mechanism of an ICME/electro-biocarriers-MBR system in livestock wastewater (antibiotic-containing) treatment. J Hazard Mater 426:128064. https://doi.org/10.1016/j.jhazmat.2021.128064

Chenoweth J, Al-Masri RA (2022) Cumulative effects of large-scale desalination on the salinity of semi-enclosed seas. Desalination 526:115522. https://doi.org/10.1016/j.desal.2021.115522

Delgado-Torres AM, García-Rodríguez L (2007a) Double cascade organic Rankine cycle for solar-driven reverse osmosis desalination. Desalination 216:306–313. https://doi.org/10.1016/j.desal.2006.12.017

Delgado-Torres AM, García-Rodríguez L (2007b) Preliminary assessment of solar organic Rankine cycles for driving a desalination system. Desalination 216:252–275. https://doi.org/10.1016/j.desal.2006.12.011

Delgado-Torres AM, García-Rodríguez L (2012) Design recommendations for solar organic Rankine cycle (ORC)–powered reverse osmosis (RO) desalination. Renew Sustain Energy Rev 16:44–53. https://doi.org/10.1016/j.rser.2011.07.135

Fang X, Wang Q, Wang J, Xiang Y, Wu Y, Zhang Y (2021) Employing extreme value theory to establish nutrient criteria in bay waters: a case study of Xiangshan Bay. J Hydrol 603:127146. https://doi.org/10.1016/j.jhydrol.2021.127146

García-Rodríguez L, Delgado-Torres AM (2007) Solar-powered Rankine cycles for fresh water production. Desalination 212:319–327. https://doi.org/10.1016/j.desal.2006.10.016

Ge D, Yuan H, Xiao J, Zhu N (2019) Insight into the enhanced sludge dewaterability by tannic acid conditioning and pH regulation. Sci Total Environ 679:298–306. https://doi.org/10.1016/j.scitotenv.2019.05.060

Geng D, Du Y, Yang R (2016) Performance analysis of an organic Rankine cycle for a reverse osmosis desalination system using zeotropic mixtures. Desalination 381:38–46. https://doi.org/10.1016/j.desal.2015.11.026

Hassan A, Elwardany AE, Ookawara S, Sekiguchi H, Hassan H (2022) Energy, exergy, economic and environmental (4E) assessment of hybrid solar system powering adsorption-parallel/series ORC multigeneration system. Process Saf Environ Prot 164:761–780. https://doi.org/10.1016/j.psep.2022.06.024

Igobo ON, Davies PA (2018) Isothermal organic rankine cycle (ORC) driving reverse osmosis (RO) desalination: experimental investigation and case study using R245fa working fluid. Appl Therm Eng 136:740–746. https://doi.org/10.1016/j.applthermaleng.2018.02.056

Ihsanullah I, Atieh MA, Sajid M, Nazal MK (2021) Desalination and environment: a critical analysis of impacts, mitigation strategies, and greener desalination technologies. Sci Total Environ 780:146585. https://doi.org/10.1016/j.scitotenv.2021.146585

(2015) Intakes and outfalls for seawater Reverse-Osmosis Desalination facilities. Environ Sci Eng https://doi.org/10.1007/978-3-319-13203-7.

Izadpanah F, Mokhtari H, Izadpanah S, Sadeghi MS (2022) Optimization of cogeneration for power and desalination to satisfy the demand of water and power at high ambient temperatures. Appl Therm Eng 216:119014. https://doi.org/10.1016/j.applthermaleng.2022.119014

Jaafari R, Rahimi A (2021) Determination of optimum organic Rankine cycle parameters and configuration for utilizing waste heat in the steel industry as a driver of receive osmosis system. Energy Rep 7:4146–4171. https://doi.org/10.1016/j.egyr.2021.06.065

JaliliJamshidian F, Gorjian S, Shafieefar M (2022) Techno-economic assessment of a hybrid RO-MED desalination plant integrated with a solar CHP system. Energy Convers Manage 251:114985. https://doi.org/10.1016/j.enconman.2021.114985

Jones E, Qadir M, van Vliet MTH, Smakhtin V, Kang S (2019) The state of desalination and brine production: a global outlook. Sci Total Environ 657:1343–1356. https://doi.org/10.1016/j.scitotenv.2018.12.076

Karellas S, Terzis K, Manolakos D (2011) Investigation of an autonomous hybrid solar thermal ORC–PV RO desalination system The Chalki island case. Renew Energy 36:583–590. https://doi.org/10.1016/j.renene.2010.07.012

Khanarmuei M, Ahmadisedigh H, Ebrahimi I, Gosselin L, Mokhtari H (2017) Comparative design of plug and recirculation RO systems; Thermoeconomic: case study. Energy 121:205–219. https://doi.org/10.1016/j.energy.2017.01.028

Khudair KM, Eraibi NA (2017) Environmental impact of RO units installation in main water treatment plants of Basrah city/south of Iraq. Desalination 404:270–279. https://doi.org/10.1016/j.desal.2016.11.020

Kosmadakis G, Manolakos D, Kyritsis S, Papadakis G (2009a) Economic assessment of a two-stage solar organic Rankine cycle for reverse osmosis desalination. Renew Energy 34:1579–1586. https://doi.org/10.1016/j.renene.2008.11.007

Kosmadakis G, Manolakos D, Kyritsis S, Papadakis G (2009b) Comparative thermodynamic study of refrigerants to select the best for use in the high-temperature stage of a two-stage organic Rankine cycle for RO desalination. Desalination 243:74–94. https://doi.org/10.1016/j.desal.2008.04.016

Kosmadakis G, Manolakos D, Papadakis G (2010a) Parametric theoretical study of a two-stage solar organic Rankine cycle for RO desalination. Renew Energy 35:989–996. https://doi.org/10.1016/j.renene.2009.10.032

Kosmadakis G, Manolakos D, Kyritsis S, Papadakis G (2010b) Design of a two stage Organic Rankine Cycle system for reverse osmosis desalination supplied from a steady thermal source. Desalination 250:323–328. https://doi.org/10.1016/j.desal.2009.09.050

Li C, Kosmadakis G, Manolakos D, Stefanakos E, Papadakis G, Goswami DY (2013a) Performance investigation of concentrating solar collectors coupled with a transcritical organic Rankine cycle for power and seawater desalination co-generation. Desalination 318:107–117. https://doi.org/10.1016/j.desal.2013.03.026

Li C, Besarati S, Goswami Y, Stefanakos E, Chen H (2013b) Reverse osmosis desalination driven by low temperature supercritical organic rankine cycle. Appl Energy 102:1071–1080. https://doi.org/10.1016/j.apenergy.2012.06.028

Li J, Zheng J, Peng X, Dai Z, Liu W, Deng H, Xi B, Lin Z (2020) NaCl recovery from organic pollutants-containing salt waste via dual effects of aqueous two-phase systems (ATPS) and crystal regulation with acetone. J Clean Prod 260:121044. https://doi.org/10.1016/j.jclepro.2020.121044

Lin X, Lu K, Hardison AK, Liu Z, Xu X, Gao D, Gong Jun, Gardner WS (2021) Membrane inlet mass spectrometry method (REOX/MIMS) to measure 15N-nitrate in isotope-enrichment experiments. Ecol Indicat 126:107639. https://doi.org/10.1016/j.ecolind.2021.107639

Manolakos D, Papadakis G, Mohamed ES, Kyritsis S, Bouzianas K (2005) Design of an autonomous low-temperature solar Rankine cycle system for reverse osmosis desalination. Desalination 183:73–80. https://doi.org/10.1016/j.desal.2005.02.044

Manolakos D, Papadakis G, Kyritsis S, Bouzianas K (2007) Experimental evaluation of an autonomous low-temperature solar Rankine cycle system for reverse osmosis desalination. Desalination 203:366–374. https://doi.org/10.1016/j.desal.2006.04.018

Manolakos D, Mohamed ES, Karagiannis I, Papadakis G (2008) Technical and economic comparison between PV-RO system and RO-Solar Rankine system. Case study: Thirasia Island. Desalination 221:37–46. https://doi.org/10.1016/j.desal.2007.01.066

Manolakos D, Kosmadakis G, Kyritsis S, Papadakis G (2009a) On site experimental evaluation of a low-temperature solar organic Rankine cycle system for RO desalination. Sol Energy 83:646–656. https://doi.org/10.1016/j.solener.2008.10.014

Manolakos D, Kosmadakis G, Kyritsis S, Papadakis G (2009b) Identification of behaviour and evaluation of performance of small scale, low-temperature Organic Rankine Cycle system coupled with a RO desalination unit. Energy 34:767–774. https://doi.org/10.1016/J.ENERGY.2009.02.008

Mansouri MT, Amidpour M, Ponce-Ortega M (2020) Optimization of the integrated power and desalination plant with algal cultivation system compromising the energy-water-environment nexus.

Sustain Energy Technol Assess 42:100879. https://doi.org/10.1016/j.seta.2020.100879
Missimer TM, Maliva RG (2018) Environmental issues in seawater reverse osmosis desalination: intakes and outfalls. Desalination 434:198–215. https://doi.org/10.1016/j.desal.2017.07.012
Mokhtari H, Bidi M, Gholinejad M (2014) Thermoeconomic analysis and multiobjective optimization of a solar desalination plant. J Sol Energy 2014:1–13. https://doi.org/10.1155/2014/892348
Mokhtari H, Ahmadisedigh H, Ebrahimi I (2016) Comparative 4E analysis for solar desalinated water production by utilizing organic fluid and water. Desalination 377:108–122. https://doi.org/10.1016/j.desal.2015.09.014
Nabati AM, Sadeghi MS, Naserabad SN, Mokhtari H, Izadpanah S (2018) Thermo-economic analysis for determination of optimized connection between solar field and combined cycle power plant. Energy 162:1062–1076. https://doi.org/10.1016/j.energy.2018.08.047
Nafey AS, Sharaf MA, García-Rodríguez L (2010) Thermo-economic analysis of a combined solar organic Rankine cycle-reverse osmosis desalination process with different energy recovery configurations. Desalination 261:138–147. https://doi.org/10.1016/j.desal.2010.05.017
Nemati A, Sadeghi M, Yari M (2017) Exergoeconomic analysis and multi-objective optimization of a marine engine waste heat driven RO desalination system integrated with an organic Rankine cycle using zeotropic working fluid. Desalination 422:113–123. https://doi.org/10.1016/j.desal.2017.08.012
Peñate B, García-Rodríguez L (2012) Seawater reverse osmosis desalination driven by a solar Organic Rankine Cycle: design and technology assessment for medium capacity range. Desalination 284:86–91. https://doi.org/10.1016/j.desal.2011.08.040
Pugsley A, Zacharopoulos A, Mondol JD, Smyth M (2016) Global applicability of solar desalination. Renew Energy 88:200–219. https://doi.org/10.1016/j.renene.2015.11.017
Quan Q, Gao S, Shang Y, Wang B (2021) Assessment of the sustainability of Gymnocypris eckloni habitat under river damming in the source region of the Yellow River. Sci Total Environ 778:146312. https://doi.org/10.1016/j.scitotenv.2021.146312
Sayyaadi H, Mehrabipour R (2012) Efficiency enhancement of a gas turbine cycle using an optimized tubular recuperative heat exchanger. Energy 38:362–375. https://doi.org/10.1016/j.energy.2011.11.048
Shahabi MP, McHugh A, Ho G (2015) Environmental and economic assessment of beach well intake versus open intake for seawater reverse osmosis desalination. Desalination 357:259–266. https://doi.org/10.1016/j.desal.2014.12.003
Shayesteh AA, Koohshekan O, Ghasemi A, Nemati M, Mokhtari H (2019) Determination of the ORC-RO system optimum parameters based on 4E analysis; Water–energy-environment nexus. Energy Convers Manag 183:772–790. https://doi.org/10.1016/j.enconman.2018.12.119
Tajik Mansouri M, Amidpour M, Ponce-Ortega JM (2019) Optimal integration of organic Rankine cycle and desalination systems with industrial processes: energy-water-environment nexus. Appl Therm Eng 158:113740. https://doi.org/10.1016/j.applthermaleng.2019.113740
Tchanche BF, Lambrinos G, Frangoudakis A, Papadakis G (2010) Exergy analysis of micro-organic Rankine power cycles for a small scale solar driven reverse osmosis desalination system. Appl Energy 87:1295–1306. https://doi.org/10.1016/j.apenergy.2009.07.011
Yang L, Guo H, Chen H, He L, Sun T (2018) A bibliometric analysis of desalination research during 1997–2012. Water Conserv Manag 2(1):18–23. https://doi.org/10.26480/wcm.01.2018.18.23
Yang Z, Yu X, Dedman S, Rosso M, Zhu J, Yang, J.,... Wang, J. (2022) UAV remote sensing applications in marine monitoring: knowledge visualization and review. Sci Total Environ 838:155939. https://doi.org/10.1016/j.scitotenv.2022.155939